

Ultraintense Laser-Produced Fast-Electron Propagation in Gas Jets

D. Batani,¹ S. D. Baton,² M. Manclossi,^{1,*} J. J. Santos,² F. Amiranoff,² M. Koenig,² E. Martinolli,^{1,2} A. Antonicci,¹
C. Rousseaux,³ M. Rabec Le Gloahec,³ T. Hall,⁴ V. Malka,⁵ T. E. Cowan,⁶ J. King,⁷ R. R. Freeman,^{7,†}
M. Key,⁸ and R. Stephens⁹

¹*Dipartimento di Fisica "G. Occhialini" and INFM, Università di Milano-Bicocca, Italy*

²*Laboratoire pour l'Utilisation des Lasers Intenses, UMR 7605 CNRS-CEA-X-Paris VI, Ecole Polytechnique, Palaiseau, France*

³*Commissariat à l'Energie Atomique, Bruyères-le-Châtel, France*

⁴*University of Essex, Wivenhoe Park, Colchester, Essex, CO4 3SQ, United Kingdom*

⁵*Laboratoire d'Optique Appliquée, UMR ENSTA-CNRS-Ecole Polytechnique, Palaiseau, France*

⁶*University of Nevada, Reno, Nevada, USA*

⁷*Department of Applied Sciences, University of California, Davis, Davis, California 95616, USA*

⁸*Lawrence Livermore National Laboratory, Livermore, California, USA*

⁹*Inertial Fusion Technology Division, Energy Group, General Atomics, San Diego, CA 92121, USA*

(Received 18 February 2004; published 9 February 2005)

We study the propagation of fast electrons in a gas at different densities. A large relativistic electron current is produced by focusing a short-pulse ultrahigh-intensity laser on a metallic target. It then propagates in a gas jet placed behind the foil. Shadowgraphy in the gas shows an electron cloud moving at sub-relativistic average velocities. The experiment shows (i) the essential role of the density of background material for allowing propagation of fast electrons, (ii) the importance of the ionization phase which produces free electrons available for the return current, and (iii) the effect of electrostatic fields on fast-electron propagation.

DOI: 10.1103/PhysRevLett.94.055004

PACS numbers: 52.38.Kd, 52.35.Vd

Introduction.—Recently much attention has been given to the generation of fast electrons in ultrahigh-intensity laser interactions and to their transport in matter [1]. The propagation of relativistic currents largely exceeding the Alfvén limit [2] and generating huge electric and magnetic fields opens new perspectives for applications such as fast ignition [3,4], and poses new physical problems. Previous experiments [5] using $K\text{-}\alpha$ spectroscopy have shown the influence of the target electric properties on fast-electron propagation. While in conductors, it was as expected on the basis of collisional effects, a reduced propagation was evidenced in insulators, in relation with the self-generated fields, an effect first predicted by Bell *et al.* [6].

Experiments on fused silica targets [7,8] with time-resolved optical shadowgraphy have shown collimated jets of fast electrons, justified by the focusing effect of self-induced magnetic fields. A larger isotropic cloud transporting the major part of the electron energy at $\approx c/2$ has been also observed. The effect of target density on electron propagation has been evidenced in experiments using $K\text{-}\alpha$ spectroscopy and foam targets [9]. This was related to the difference in conductivity for different heatings induced by the fast-electron propagation [9,10].

Recent experiments have shown how the passage of fast electrons at the target-vacuum interface on the target rear side produces significant optical transition radiation (OTR) [11]. Also, the emission of coherent OTR at the laser harmonics [12] has evidenced that part of the fast electrons are produced and propagate ballistically in short bunches. Other experiments [13,14] have addressed the problem of target heating and electron beam geometry, through $K\text{-}\alpha$

spectroscopy and $K\text{-}\alpha$ imaging. Finally, Tatarakis *et al.* [15] studied electron propagation in a gas target by using optical shadowgraphy. Although the experimental setup and the experimental conditions presented in [15] are similar to those described in the present Letter, the goal of their experiment was different from ours. While they have studied small-scale filamentation using a large magnification, we looked at the *global* electron propagation on a larger spatial scale. Following the results presented here, it could appear that the filamentation observed by Tatarakis *et al.* does not affect fast-electron transport dramatically.

Many theoretical and numerical works addressed the mechanisms involved in fast-electron propagation at currents above the Alfvén limit. The necessity of current neutralization as well as charge neutralization explains the dramatic effect on the propagation of the density of free electrons in the medium. This qualitatively explains the differences observed between insulators and conductors: in insulators, free electrons need to be created by field or impact ionization, processes which require time and energy. This results in stronger fields and a more inhibited motion. As for the nature of fields producing inhibition, Bell *et al.* [6] consider an electrostatic field. Tikhonchuk [16] explicitly calculates charge separation and electrostatic fields through Poisson equation. However, most computer models [17–19] neglect electrostatic fields; inductive fields play the main role, a reasonable assumption in conductors but probably not in insulators.

In this context we made an experiment where we first generate fast electrons by irradiating a thin metallic (Ti) target with a high-intensity short-pulse laser beam before

propagating them in a gas jet (Ar or He) at different densities. A second foil (Al) located behind the jet gave the possibility for additional diagnostics ($K\text{-}\alpha$, OTR). Advantages of using a gas are: (i) density can easily be changed by adjusting the pressure; (ii) gases are optically transparent so that optical shadowgraphy can be used as a diagnostic tool; (iii) a gas, as foams, fused silica and plastic, is an insulator, implying the need for ionization; (iv) very low densities can be used, thus maximizing inhibition; this offers a unique possibility of studying inhibition when it is not *marginal*.

Also, the gas medium is practically noncollisional for fast electrons, hence the main effect on propagation is due to self-generated fields. Finally, it should be noted that, in fast ignition, the deposition of 10 kJ in ≈ 10 ps over $\approx 10 \mu\text{m}$ [3] implies fast-electron densities $n_b \approx 10^{23} \text{ cm}^{-3}$. While at present it is not clear how these can be generated, still such densities are much larger than in typical coronal plasmas ($n_e \approx 10^{21} \text{ cm}^{-3}$). Hence the study of the limit $n_b \geq n_e$ is also of *practical* importance for fast ignition. This limit is indeed also met in our experiment: we recall that typical fast-electron energy of ≈ 1 MeV, and conversion efficiencies from laser energy to fast electrons up to $\approx 15\%$ – 25% , have been measured with our setup [5,11,12]. Since the electron beam is produced from a region comparable to the focal spot in a time of the order of the laser pulse duration, we get $n_b \approx 5 \times 10^{20} \text{ cm}^{-3}$ (as expected, of the order of the laser critical density), while the atomic gas densities used in the experiment are $\leq 3 \times 10^{19} \text{ cm}^{-3}$, as shown later.

Experiment.—The experiment was performed with the LULI 100 TW laser (350 fs, $1.057 \mu\text{m}$, energy up to 10 J) focused by a $f/3$ off-axis parabola at normal incidence on the target. The spot diameter was $\leq 15 \mu\text{m}$ giving intensities $\leq 5 \times 10^{19} \text{ W/cm}^2$. A probe beam (528 nm, 400 fs) was used for shadowgraphy, allowing 2D transverse imaging on a charge coupled device (CCD), with resolutions of $\approx 5 \mu\text{m}$ and ≈ 400 fs. The ionized region deflects the probe beam outside of the collecting optics so that by varying the time delay between the probe and the main beam, the ionization dynamics within the gas can be followed. The $K\text{-}\alpha$ and OTR diagnostics are described in [11,13]. The experiment scheme is shown in Fig. 1.

The gas atomic density in the position where the chirped pulse amplified (CPA) laser beam was focused (1.2 mm from the nozzle) was measured by an interferometric diagnostic in conditions similar to the experiment.

Figure 2 is a typical shadowgraphy image showing two different structures: (i) a large cloud and (ii) straight lines probably connected to *electron jets*. Such jets could be due to the *first* fast electrons, arriving to the rear of the first foil and propagating in the gas before a large field has developed. Hence they are not too important in fast-electron transport and this Letter will mainly focus on the cloud.

As for other diagnostics, OTR shows a large emission area (up to 1 mm), after the second foil, of the same order than the large cloud at late times (see Fig. 3). Inside this

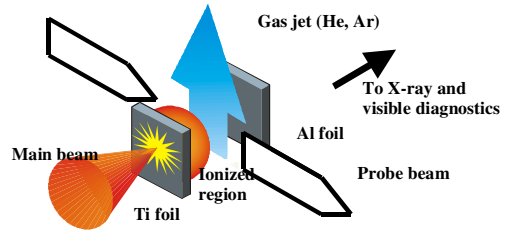


FIG. 1 (color online). Schematic experimental setup. The distance between the foils is 1.2 mm. Thickness is $20 \mu\text{m}$ (Ti) and $15 \mu\text{m}$ (Al).

emission area, images with larger magnification show small, localized emitting regions ($< 50 \mu\text{m}$), probably connected to electron jets. Also, OTR emission is strongly reduced when electrons propagate through the gas: emission from the rear of a simple foil is ≈ 100 times that from the second foil of a foil-gas-foil package. With no gas (propagation in vacuum), intensity is further reduced, but only by a factor of about two. X-ray diagnostics did not show any signal above noise from the second foil.

Figure 4 shows shadowgrams obtained at different delays between main and probe pulse. The cloud evolution can be followed and its velocity measured. Also, the smallest *cloudy* region (at early times) is always at least $\geq 150 \mu\text{m}$ in size, much larger than the focal spot or what expected from previous experiments using OTR [11] or $K\text{-}\alpha$ imaging [14]. At late times, the size is comparable to the separation between the two foils (1.2 mm). The size of the cloud in the direction perpendicular to the target surface is shown in Fig. 5 where the lines are linear interpolations giving the average cloud velocity (the expansion average velocity in transverse direction is $\approx 2\text{--}3$ times smaller). All lines start from 0 at time 0 (roughly corresponding to the arrival of the main beam on target). The average velocities in Fig. 5 are different for the four cases studied and quite slow ($c/30$ to $c/10$). Also, experimental data, especially the series at He 30 bar extending to larger delays, suggest that cloud expansion starts faster and slows down in time. However, we did not attempt to model such deceleration because our data are too scarce to support fits other than linear.

Discussion.—In our conditions, fast-electron propagation is mainly dominated by the need for a neutralizing

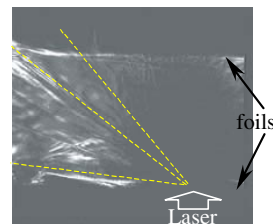


FIG. 2 (color online). Shadowgraphy image: Ar 70 bar, $\Delta t \approx 30$ ps. Dashed lines show a few of the observed straight lines probably connected to electron jets.

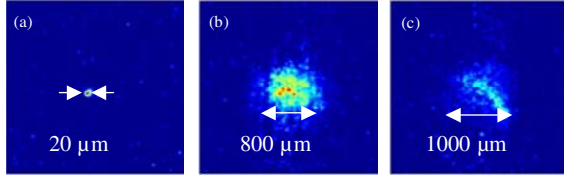


FIG. 3 (color online). Images of the target rear side obtained with the streak camera in “gated” mode. (a) Simple target, 75 μm Al; (b) Ti/He 30 bar/Al ($n_{\text{gas}} \approx 8 \cdot 10^{18} \text{ cm}^{-3}$); (c) Ti/vacuum/Al. The total emitted energy in (a) is $\approx 100 \times$ that in (b), and $200 \times$ that in (c).

return current and by the creation of electrostatic fields due to charge separation. Let us first discuss what happens at the foil-gas interface. The condition on current neutralization of fast-electron and return current is

$$J_{\text{TOT}} = en_b v_b - en_e v_e \approx 0, \quad (1)$$

and since v_e cannot be $> c$, it follows that (i) the maximum fast-electron current density which can propagate is $en_e c$, and (ii) background electrons are also accelerated to high velocities in our conditions (hence speaking of *fast* and *slow* electrons is no longer correct). The condition in Eq. (1) also explains why the cloud minimum size is large. When fast electrons reach the rear side of the thin foil, their density is high, their current cannot be compensated, and they cannot penetrate the gas. Only a few escape, setting up an electrostatic field which completely stops most of the other fast electrons (until ions are also set in motion). These are effectively confined in the target and either *reflux* [14] or move along the rear surface, leading to a density reduction, until n_b is of the order of n_e in the background gas. A final beam radius in agreement with the observed size can then easily be calculated.

When fast electrons start to propagate in the gas, their motion will be dominated by charge separation. In this case, we have developed a simple model (details to be published elsewhere) which is inspired by Tikhonchuk’s work [16], but differs in the sense that Ref. [16] studies the case of solids ($n_e \gg n_b$), which implies small charge separation, relatively small fields, and weak inhibition. Then the beam velocity v_b is not too different from c . In our case, on the contrary, the fast-electron density, as generated in the foil, is much larger than the background gas density. In this case neutrality is violated at the leading edge of the propagation over the Debye length of the fast electrons.

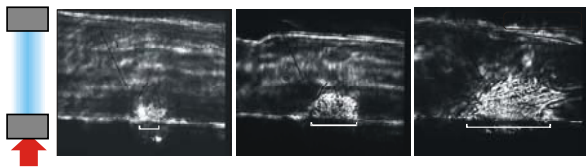


FIG. 4 (color online). Evolution of the electron cloud (He, 30 bar). From left: $\Delta t \approx 10 \text{ ps}$, $\approx 16 \text{ ps}$, $\approx 50 \text{ ps}$. Bars are 280, 540, and 1000 μm . The lower and upper dark part in all images, respectively, represent the Ti and Al foils.

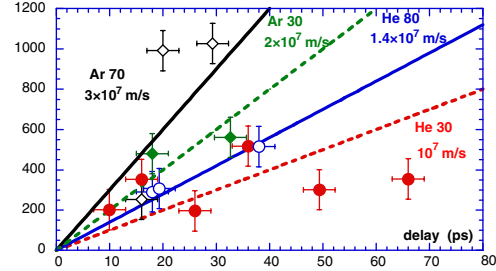


FIG. 5 (color online). Cloud dimension in μm vs time delay between main and probe pulses. Atomic densities corresponding to pressures are 10^{19} cm^{-3} (He 30 bar, full circles), $3.2 \cdot 10^{19} \text{ cm}^{-3}$ (He 80 bar, empty circles), 10^{19} cm^{-3} (Ar 30 bar, full diamonds), $2.8 \cdot 10^{19} \text{ cm}^{-3}$ (Ar 70 bar, empty diamonds).

This is also the region where the space charge electric field is large and can ionize the background gas and thus coincides with the width of the ionization front Δx (although this result sounds *usual*, we stress that it is only derived in the limit of low background densities; indeed Tikhonchuk derives a different expression for Δx). We also get the usual ambipolar expression for the electrostatic field

$$E \approx (kT_{\text{hot}} n_b / \epsilon_0)^{1/2}, \quad (2)$$

which, in our experimental conditions, can easily reach $\approx 10^{12} \text{ V/m}$. Such an electric field very rapidly ionizes the background gas, creating the free electrons which are needed for the neutralizing return current. The ionization time can be calculated by using the well known Keldish’s formula [20] as $t = 1/\nu(E)$ (Keldish’s ionization frequency). Notice that such ionization rate only depends on the strength of the electric field. However, we get a dependence on density through Eq. (2).

Although the ionization phase is very rapid, nevertheless it is fundamental, not only to create free electrons, but also to fix the background density. The huge electrostatic fields arising in the gas only exist over a distance λ_D and for a time $t_E < \lambda_D/v_{\text{cloud}}$ (typically $\lambda_D/(c/20) \approx 6 \times 10^{-14} \text{ s}$). It turns out that in our conditions, reachable ionization stages in a time t_E are Ar^{6+} and He^{2+} .

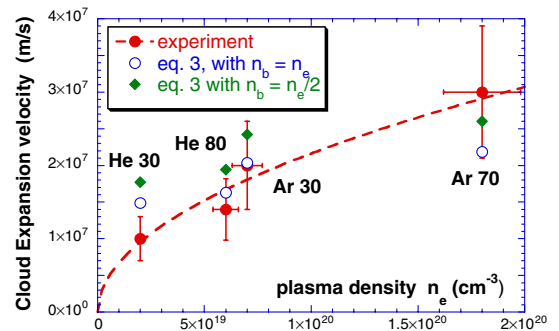


FIG. 6 (color online). Experimental and calculated cloud expansion velocity v_{cloud} vs background plasma density. We used $n_b = n_e$ (empty circles) and $n_b = n_e/2$ (full diamonds) in Eq. (3) to show the effects of density variations.

Finally, free electrons are set in motion and establish a return current which cancels the fast-electron current. Here we have another big difference with the case studied by Tikhonchuk. Indeed, for the drift velocity v_e of return electrons, he uses Drude's model (or Ohm's law for conductors), which gives a linear dependence of v_e on E . In the present strong-field limit, we find that v_e depends on the square root of E , as

$$v_e \approx (eE\lambda_{ii}/m_e)^{1/2}, \quad (3)$$

where λ_{ii} is the interionic distance in the material. The same kind of dependence was originally derived by Landau and Lifshitz [21] in the limit of strong fields.

The establishment of the return current and the cancellation of the positive charge left behind by the fast electrons takes a time of the order of $\approx \lambda_D/v_e$, where v_e is the drift velocity, given in our model by Eq. (3). This process is slow because the free background electrons are (at least initially) slow and strongly collisional, and collisions inhibit the return current. Since, however, no further propagation of the fast electrons is possible before the charge separation is cancelled, the fast-electron current is finally forced to move with a velocity close to the return velocity of background electrons, i.e., $v_{\text{cloud}} \approx v_e$. This gives a slow velocity and a strongly inhibited propagation. OTR images from the second foil confirm this strong inhibition.

Let us also notice that the average expansion velocities in Fig. 5 scale with the background density n_e (and increase with density) irrespective of gas type. Figure 6 shows experimental (Fig. 5) and calculated [Eq. (3)] cloud expansion velocities as function of background plasma density. Despite the simplicity of our model (and taking into account the large error bars which result from the large scattering of the data in Fig. 5), we get a very good qualitative and quantitative agreement.

We should also wonder about energy loss in a gas medium which is noncollisional (over our distances) for fast electrons. OTR and $K\text{-}\alpha$ results show that not many electrons reach the second foil, or at least they are no longer *energetic*. Indeed the energy spent in ionizing a gas region as large as ≈ 1.2 mm may be comparable to that in fast electrons ($\leq 25\%$ of laser energy). Also the electrostatic field itself is an efficient loss mechanism, stopping all fast electrons involved in the charge separation process in a distance $\approx \lambda_D$. Simple calculations show how these effects may completely deplete the fast-electron beam energy. Hence they provide effective mechanisms for cloud deceleration, as previously noticed.

Conclusions.—This experiment shows several novel results: (i) the background density determines the fast-electron propagation. Smaller densities correspond to weaker return currents and more inhibited motion. Our results agree with those in [7] where a velocity $\approx c/2$ was measured in dense media (however, quantitatively, these experiments, with $n_b \ll n_e$, fall in a different regime). (ii) The ionization phase is essential for producing free electrons for the return current. In our conditions, field-

ionization is dominant. (iii) Electrostatic fields are fundamental in fast-electron propagation. They drive the free electrons to *return* with a velocity determined by field strength and by the number of collisions (i.e., by gas density). Let us notice that experiments on propagation of currents above the Alfvén limit were done in the 1970s with conventional plasma apparatus [22]. However, here, currents are larger (up to 10^{13} A/cm², probably the largest ever produced), and time scales much shorter. This implies that field ionization of background material is dominant, while in [22] ionization was due to collisions only.

Part of the work was supported by the E. U. Contracts: LULI ACCESS HPRI-1999-CT 00052 and TMR ERBFMGE-CT95-0044 and by Grant No. E1127 from Région Ile-de-France. One of us (J.J.S.) was financed by MCT (Portugal) under the Contract No. PRAXIS XXI BD/18108/98. We acknowledge the help from LULI technical staff in the experiment and very useful discussions with V. Tikhonchuk, J.C. Adam, A. Héron, M. Lontano, M. Passoni, J. Honrubia, L. Gremillet, and F. Cornolti.

*Also at Dipartimento di Ingegneria Nucleare, Politecnico di Milano, Italy.

†Also at Ohio State University, Columbus, OH, USA.

- [1] R. Snavely *et al.*, Phys. Rev. Lett. **85**, 2945 (2000); M. Tatarakis *et al.*, Phys. Rev. Lett. **81**, 999 (1998); F.N. Beg *et al.*, Phys. Plasmas **4**, 447 (1997); M. Key *et al.*, Phys. Plasmas **5**, 1966 (1998); K. Wharton *et al.*, Phys. Rev. Lett. **81**, 822 (1998); T. Hall *et al.*, Phys. Rev. Lett. **81**, 1003 (1998).
- [2] H. Alfvén, Phys. Rev. **55**, 425 (1939).
- [3] M. Tabak *et al.*, Phys. Plasmas **1**, 1626 (1994).
- [4] S. Atzeni, Phys. Plasmas **6**, 3316 (1999).
- [5] F. Pisani *et al.*, Phys. Rev. E **62**, R5927 (2000).
- [6] A. Bell *et al.*, Plasma Phys. Controlled Fusion **39**, 653 (1997).
- [7] L. Gremillet *et al.*, Phys. Rev. Lett. **83**, 5015 (1999).
- [8] M. Borghesi *et al.*, Phys. Rev. Lett. **83**, 4309 (1999).
- [9] D. Batani *et al.*, Phys. Rev. E **65**, 066409 (2002).
- [10] J. Davies, Phys. Rev. E **68**, 056404 (2003).
- [11] J.J. Santos *et al.*, Phys. Rev. Lett. **89**, 025001 (2002).
- [12] S.D. Baton *et al.*, Phys. Rev. Lett. **91**, 105001 (2003).
- [13] E. Martinolli *et al.*, Laser Part. Beams **20**, 171 (2002).
- [14] R.B. Stephens *et al.*, Phys. Rev. E **69**, 066414 (2004).
- [15] M. Tatarakis *et al.*, Phys. Rev. Lett. **90**, 175001 (2003).
- [16] V.T. Tikhonchuk, Phys. Plasmas **9**, 1416 (2002).
- [17] J.R. Davies *et al.*, Phys. Rev. E **56**, 7193 (1997).
- [18] J.J. Honrubia *et al.*, Laser Part. Beams **22**, 129 (2004).
- [19] L. Gremillet *et al.*, Phys. Plasmas **9**, 941 (2002).
- [20] M.V. Ammosov, N.B. Delone, and V.P. Krainov, Sov. Phys. JETP **64**, 1191 (1986).
- [21] L.D. Landau, E.M. Lifshitz, and L.P. Pitaevskii, *Physical Kinetics*, Course of Theoretical Physics Vol. 10 (Butterworth-Heinemann, Burlington, MA, 1981), Chap. 2.
- [22] C.L. Olson, Phys. Fluids **18**, 585 (1975); Phys. Rev. A **11**, 288 (1975); **9**, 2631 (1974); D. McArthur *et al.*, Phys. Rev. Lett. **27**, 1765 (1971); J.W. Poukey *et al.*, Plasma Phys. **13**, 897 (1971).